Nuclear Medicine and Biology 71 (2019) 54–64

Contents lists available at ScienceDirect

Nuclear Medicine and Biology

journal homepage: www.elsevier.com/locate/nucmedbio

Optimization of solid-phase extraction (SPE) in the preparation of [^{18}F]D3FSP: A new PET imaging agent for mapping Aβ plaques

Xinyue Yao [a,b], Zhihao Zha [b], Ruiyue Zhao [a,b], Seok Rye Choi [c], Karl Ploessl [c], Futao Liu [a], Lin Zhu [a], Hank F. Kung [b,c,*]

[a] Key Laboratory of Radiopharmaceuticals, Ministry of Education, College of Chemistry, Beijing Normal University, Beijing 100875, PR China
[b] Department of Radiology, University of Pennsylvania, Philadelphia, PA 19104, USA
[c] Five Eleven Pharma Inc., Philadelphia, PA 19104, USA

ARTICLE INFO

Article history:
Received 11 March 2019
Received in revised form 9 May 2019
Accepted 9 May 2019
Available online xxxx

Keywords:
Alzheimer's disease
Brain imaging
Deuterium
Radiosynthesis
Solid-phase extraction

ABSTRACT

Introduction: Alzheimer's disease is a common neurodegenerative disease that is characterized by the presence of Aβ plaques in the brain. The FDA has approved the use of Amyvid (florbetapir f18, AV-45) as a PET imaging agent for detecting Aβ plaques in the living human brain. In an attempt to reduce *N*-demethylation *in vivo* by taking advantage of more stable C-D bonds, an analog of AV-45, [^{18}F]D3FSP ([^{18}F]**7**), was synthesized to improve image contrast for detecting and monitoring the Aβ plaques. A convenient and improved preparation of [^{18}F]D3FSP ([^{18}F]**7**) is needed for widespread clinical application. We report herein the optimization of the radiosynthesis and solid-phase extraction (SPE) procedure.

Methods: Radiosyntheses of [^{18}F]D3FSP ([^{18}F]**7**) under different fluorination conditions were evaluated, and the intermediate, containing an *N*-Boc protecting group, was deprotected using different acids. One of the major objectives was to simplify the final purification step *via* SPE to avoid the commonly employed HPLC purification and maximize the radiochemical yields of [^{18}F]D3FSP ([^{18}F]**7**) while simultaneously removing several chemical impurities (pseudocarriers). Washing various solid-phase cartridges with different combinations of ethanol/water and acetonitrile/water was explored to optimize the purification step. To evaluate the potential interference in Aβ plaques imaging from the presence of pseudocarriers, each chemical was identified and quantified by LC/MS and HPLC. An *in vitro* binding assay was employed to evaluate the binding affinities of [^{18}F]D3FSP ([^{18}F]**7**) and the pseudocarriers to Aβ plaques using postmortem AD brain tissue.

Results: Using the optimized radiosynthesis method and SPE purification, the final dose of [^{18}F]D3FSP ([^{18}F]**7**) was obtained in 50 min with a very low content of pseudocarriers (21.7 ± 5.5 μg). The radiochemical yield was 44.4 ± 5.7% (decay corrected), and the radiochemical purity was >95%. SPE-purified doses of [^{18}F]D3FSP ([^{18}F]**7**) displayed excellent binding affinity and specificity for Aβ plaques as measured in an *in vitro* binding assay using AD brain homogenates, and the OH-pseudocarrier, **8** (K_i = 19.5 ± 0.5 nM), and the Cl-pseudocarrier, **10** (K_i = 18.6 ± 3.9 nM), showed lower binding affinities for Aβ plaques than those of AV-45 (K_i = 8.6 ± 0.5 nM) and D3FSP, **7** (K_i = 9.8 ± 0.5 nM).

Conclusions: An optimized radiosynthesis and fast SPE purification method suitable for the preparation of clinical doses of [^{18}F]D3FSP ([^{18}F]**7**) was accomplished. The results of quality control tests and binding studies suggested that the SPE-purified doses of [^{18}F]D3FSP ([^{18}F]**7**) are appropriate for imaging Aβ plaques in the human brain.

Abbreviations: AD, Alzheimer's disease; Aβ, β-Amyloid; PET, Positron emission tomography; PIB, Pittsburgh compound B; SB-13, 4-*N*-Methylamino-4′-hydroxystilbene; [^{18}F]AV-45, [^{18}F]Florbetapir f 18; [^{18}F]AV-1, [^{18}F]Florbetaben f 18; [^{18}F]GE-067, [^{18}F]Flutemetamol f 18; [^{18}F]NAV4694, 2-(2-([^{18}F]Fluoro)-6-methylaminopyridin-3-yl)benzofuran-5-ol; [^{18}F]FC119S, (*R*)-1-(Fluoro-^{18}F)-3-((2-(6-(methylamino)pyridin-3-yl)benzo[*d*]thiazol-6-yl)oxy)propan-2-ol; FDA, U.S. Food and Drug Administration; [^{18}F]AV-160, (*E*)-4-(2-(6-(2-(2-(2-(Fluoro-^{18}F)ethoxy)ethoxy)ethoxy)pyridin-3-yl)vinyl)aniline; SD809, Deutetrabenazine; (*S,S*)-[^{18}F]FMeNER-D2, (*S*)-2-((*S*)-2-((Fluoro-^{18}F)methoxy-D2)phenoxy)(phenyl)methyl)morpholine; NET, Norepinephrine transporter; MAO-B, Monoamine oxidase B; [^{18}F]D6-FP-()- DTBZ, (*2R,3R,11bR*)-9-(3-(Fluoro-^{18}F)propoxy-1,1,2,2,3,3-D6)-3-isobutyl-10-methoxy-1,3,4,6,7,11b-hexahydro-2H-pyrido[2,1-*a*]isoquinolin-2-ol; VMAT2, Vesicular monoamine transporter 2; [^{18}F]D12FPBM, 2-((2-((Bis(methyl-D3)amino)methyl)-4-(3-(fluoro-^{18}F)propoxy-1,1,2,2,3,3-D6)phenyl)thio)aniline; HPLC, High-performance liquid chromatography; SPE, Solid-phase extraction; FDG, Fluorodeoxyglucose; FC, Flash chromatography; TLC, Thin-layer chromatography; DMSO, Dimethyl sulfoxide; K222, Kryptofix 222; DMF, *N,N*-Dimethylformamide; DMA, *N,N*-Dimethylacetamide; AFB, Ammonium formate buffer; ACN, Acetonitrile; RCY, Radiochemical yield; RCP, Radiochemical purity; IMPY, 6-Iodo-2-(4′-*N,N*-dimethylamino)-phenylimidazo[1,2-*a*]pyridine; EtOH, Ethanol.

* Corresponding author at: Department of Radiology, University of Pennsylvania, Philadelphia, PA 19104, USA.
E-mail address: kunghf@gmail.com (H.F. Kung).

https://doi.org/10.1016/j.nucmedbio.2019.05.002
0969-8051/

1. Introduction

Alzheimer's disease (AD), a neurodegenerative disease, is characterized by progressive memory loss and cognitive impairment and has become a major public health concern worldwide. It is not clear what causes AD, but deposition of β-amyloid (Aβ) peptide and neurofibrillary tangles are pathological hallmarks of AD. According to the amyloid hypothesis, the accumulation of Aβ peptides in the brain is a defining pathologic feature in the pathogenesis of AD. Currently, the definitive method for diagnosing AD requires postmortem histopathology to demonstrate the presence of Aβ plaques in the brain [1–6]. Position emission tomography (PET) is a useful *in vivo* imaging tool for mapping Aβ plaques in the brain of AD patients [7,8]. Therefore, the development of Aβ plaque imaging probes for the early diagnosis of AD and evaluation of treatment efficacy has been one of the most attractive challenges in the field of brain imaging over the past fifteen years [9–11]. The recently reported "NIA-AA Research Framework: Toward a biological definition of Alzheimer's disease" suggested using biological definitions, such as PET imaging of Aβ plaques in the brain, instead of clinical neurological observations to define the presence of AD [12,13]. This advancement using PET imaging of AD biomarkers, *i.e.*, Aβ plaques in the brain, will likely improve the diagnosis of AD [14] and further facilitate the development of therapeutic agents [15,16].

A diverse group of core structures have been reported, including PIB and SB-13, which are labeled with ^{11}C, and AV-45 (florbetapir f18, Amyvid), AV-1 (florbetaben f18, NeuraCeq), GE-067 (flutemetamol f18, Vizamyl), NAV4694 and FC119S, which are labeled with ^{18}F. Among them, [^{18}F]AV-45 (florbetapir f18, Amyvid), [^{18}F]AV-1 (florbetaben f18, NeuraCeq), and [^{18}F]GE-067 (flutemetamol f18, Vizamyl) have been commercially developed and approved by the U.S. Food and Drug Administration (FDA) for detecting Aβ plaques in the brain (Fig. 1) [17–23]. [^{18}F]AV-45, first approved in 2012, demonstrated high binding affinity for Aβ plaques in the brain and could be useful for monitoring Aβ plaques, following disease progression and providing further evidence for therapeutic intervention in AD patients [24–28]. One of the major metabolites of [^{18}F]AV-45 ($K_i = 2.87 \pm 0.17$ nM) is the *N*-demethylated product, [^{18}F]AV-160 ($K_i = 54 \pm 5$ nM, Fig. 2). This metabolite, formed in the peripheral system, can cross the blood-brain barrier and displays high affinity for Aβ plaques, increasing the total nonspecific binding in the image. The *in vivo* metabolism of [^{18}F]AV-45 in humans may reduce the plasma concentration of the radiotracer available for binding to Aβ plaques in the brain [29,30]. Therefore, slowing *in vivo* metabolism might improve brain retention and reduce nonspecific binding.

Replacement of the hydrogen atoms in the *N*-methyl group with deuterium atoms might increase drug stability by reducing the rates of enzymatic metabolism [31–33]. The FDA recently approved deuterated tetrabenazine (SD-809, Austedo) for the treatment of Huntington's disease [34]. In the past few decades, there have been a number of reports on using deuterium/hydrogen substitution to improve the *in vivo* stability of PET imaging agents. (*S,S*)-[^{18}F]FMeNER-D2 showed excellent pharmacokinetic properties for clinical norepinephrine transporter (NET) imaging [35]. [^{18}F]Fluororasagiline-D2 and [^{18}F]fluorodeprenyl-D2, both used for mapping monoamino oxidase B (MAO-B) distribution in the human brain, are successful examples of enhanced metabolic stability by incorporating carbon-deuterium bonds [36]. In addition, [^{18}F]D6-FP-( )-DTBZ, for vesicular monoamine transporter 2 (VMAT2) imaging, and [^{18}F]D12FPBM, for serotonin transporter imaging, have also been reported (Fig. 3) [37,38].

In an attempt to reduce the formation of the *N*-demethylated product *in vivo* by taking advantage of more stable carbon-deuterium bonds, we designed a deuterated *N*-methyl derivative of AV-45, namely, D3FSP, **7**. We hypothesize that [^{18}F]D3FSP ([^{18}F]**7**) might display a similarly high binding affinity for Aβ plaques in the human brain while being metabolized more slowly in the peripheral organs, avoiding increased nonspecific signals in the brain.

In the package inserts of the three FDA-approved AD imaging agents, the recommended chemical doses for [^{18}F]AV-45 (florbetapir, Amyvid), [^{18}F]AV-1 (florbetaben, NeuraCeq), and [^{18}F]GE-067 (flutemetamol, Vizamyl) are in "mass doses" no higher than 50 μg, 30 μg and 20 μg, respectively [39]. High specific activity (SA) is critical for AD imaging. Semipreparative high-performance liquid chromatography (HPLC) is generally used for improving chemical and radiochemical purities in the preparation of radiotracers. In addition, the synthesis of radiopharmaceuticals for PET requires short reaction times, simple manipulations and facile purifications due to the short-lived radionuclides, such as ^{11}C ($t_{1/2} = 20.3$ min) and ^{18}F ($t_{1/2} = 109.8$ min) [40,41]. In an attempt to simplify the preparation process, solid-phase extraction (SPE) for the purification of [^{18}F]FDG was reported and used in routine clinical applications, and this method avoided time-consuming HPLC purifications [42,43]. In recent years, SPE has been widely used in the purification and formulation of radiopharmaceuticals, including [^{11}C]MTO, [^{18}F]FET and [^{18}F]FMZ [44–46]. The SPE purification of [^{18}F]AV-45 has been evaluated and reported. [^{18}F]AV-45 was prepared on a radiosynthesis

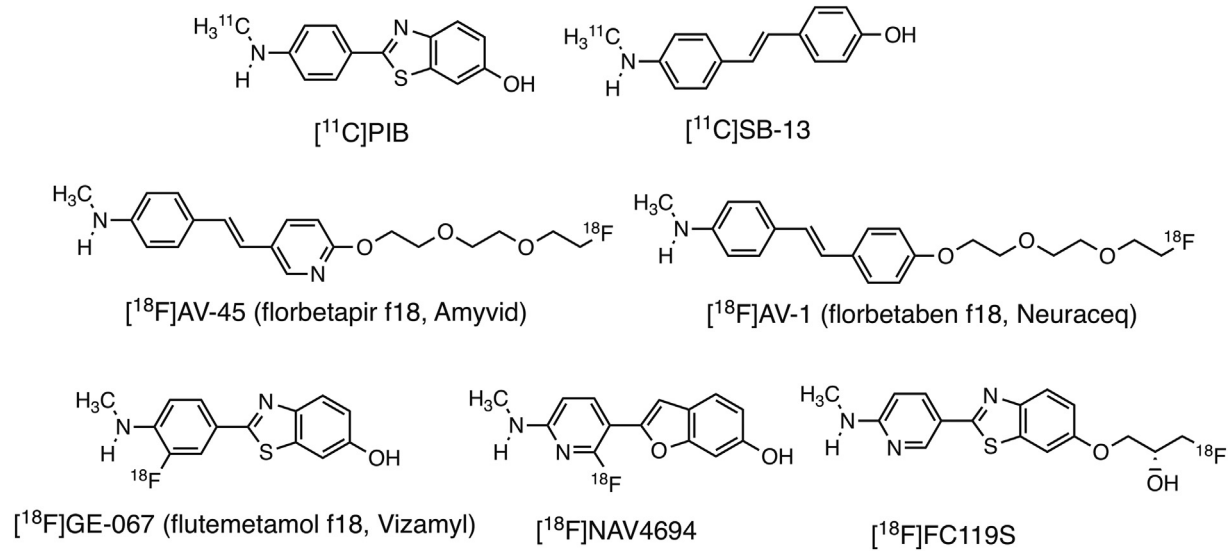

Fig. 1. Chemical structures of reported PET imaging agents for Aβ plaques in the brain. Among them, [^{18}F]AV-45 (florbetapir f18, Amyvid), [^{18}F]AV-1 (florbetaben f18, NeuraCeq) and [^{18}F]GE-067 (flutemetamol f18, Vizamyl) have been approved by the FDA.

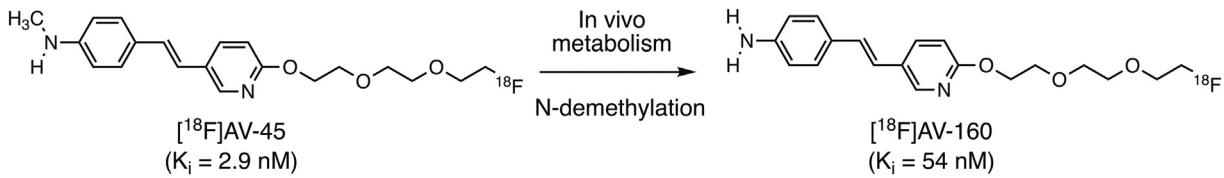

Fig. 2. The *N*-demethylated product, [^{18}F]AV-160, is one of the major metabolites of [^{18}F]AV-45 (Amyvid) in human blood. It shows a lower binding affinity for Aβ plaques in the brain and likely contributes to increased nonspecific binding.

module and purified with a SPE cartridge (Oasis HLB) with a non-decay-corrected yield of 33.6 ± 5.2%, while 510 ± 162 μg of the OH-pseudocarrier remained after preparation [47], and this yield was higher than the total mass of chemical (50 μg) recommended in the package insert.

To facilitate clinical trials and future applications of [^{18}F]D3FSP ([^{18}F]**7**), our efforts are focused on (1) optimizing the radiosynthesis and (2) using SPE purification instead of HPLC purification to reduce the amounts of chemical impurities (total mass of chemical below 50 μg per synthesis batch) and simplify the preparation process. Washing various solid-phase cartridges with different combinations of ethanol/water (EtOH/H_2O) or acetonitrile/water (ACN/H_2O) was explored to optimize the purification step. To evaluate the potential interference in Aβ plaque imaging from the presence of pseudocarriers, each chemical was identified and quantified by LC/MS and HPLC. An *in vitro* binding assay was employed to evaluate the binding affinities of [^{18}F]D3FSP ([^{18}F]**7**) and the pseudocarriers for Aβ plaques using postmortem AD brain homogenates.

2. Experimental section

2.1. General

All reagents and solvents used were commercial products and were used without further purification unless otherwise indicated. Generally, crude compounds were purified by flash chromatography (FC) using silica gel (Aldrich). ^{1}H NMR, ^{13}C NMR and ^{19}F NMR spectra were obtained on a Bruker AVANCE II 400 Spectrometer at 400, 100 and 376.5 MHz, respectively. Chemical shifts are reported in units of parts per million (ppm, δ) with the coupling constant, *J*, in Hz. The multiplicities are given as singlet (s), doublet (d), triplet (t), broad (br) or multiplet (m). High-resolution mass spectrometry (HRMS) data were obtained with an Agilent (Santa Clara, CA) G3250AA LC/MSD TOF system. Thin-layer chromatography (TLC) separations were performed using Merck silica gel 60 F 254 plates. SPE cartridges were purchased from Waters and Macherey Nagel. Postmortem AD human samples were obtained from the National Disease Research Interchange (NDRI, Philadelphia, PA, USA).

2.2. Chemistry

AV-45 and [^{18}F]AV-45 were prepared as previously reported [48,49].

2-(2-(2-((5-Iodopyridin-2-yl)oxy)ethoxy)ethoxy)ethan-1-ol (1) and ***tert*-butyl (4-vinylphenyl)carbamate (2)** were prepared as previously reported [50].

2.2.1. tert-Butyl(methyl-D3)(4-vinylphenyl)carbamate (3)

To a solution of *p*-(*tert*-butoxycarbonylamino)styrene (**2**, 2.19 g, 10 mmol) in 15 mL of DMF was slowly added a 60% NaH dispersion in mineral oil (60%, 600 mg, 15 mmol). After stirring at room temperature (rt) for 0.5 h, deuterated iodomethane (2.90 g, 20 mmol) was added. The reaction mixture was stirred at rt for 2 h, and then the reaction

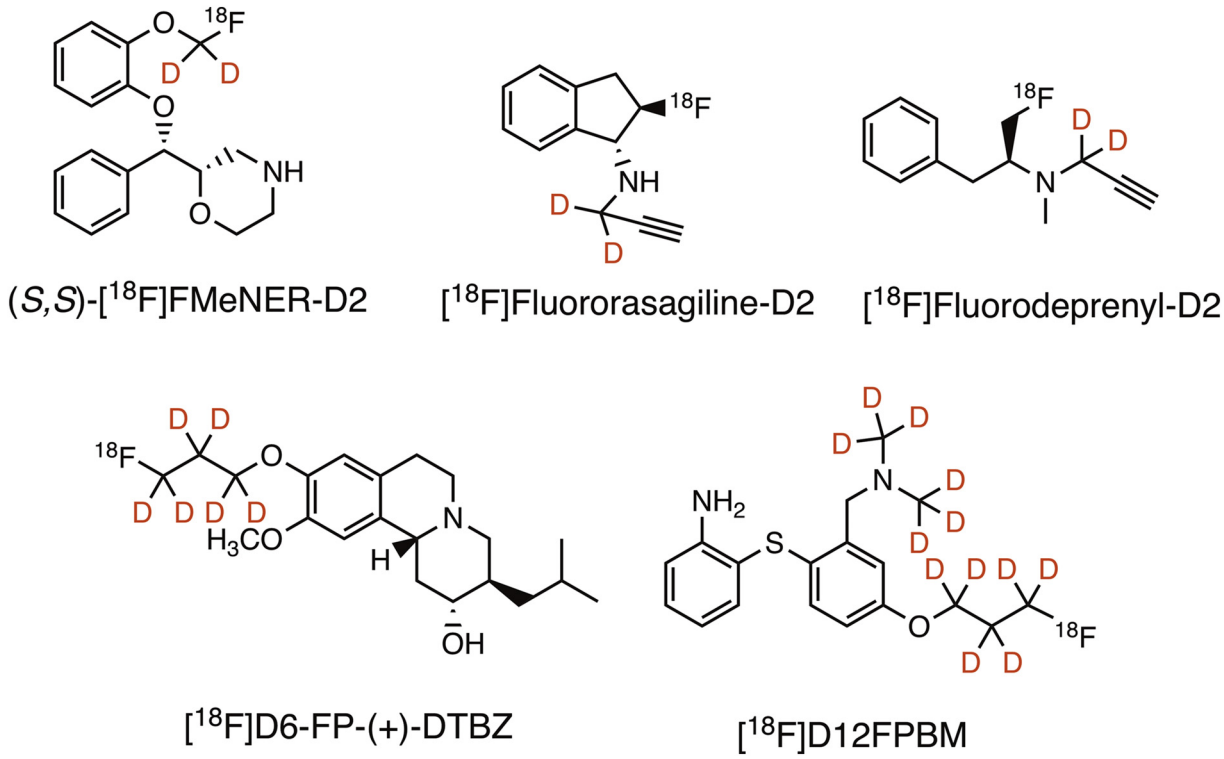

Fig. 3. Chemical structures of deuterated PET imaging agents.

mixture was quenched with 40 mL of saturated ammonium chloride (NH_4Cl) solution at 0 °C. The mixture was then extracted with 60 mL of EtOAc. The organic layer was washed with H_2O as well as brine (40 mL), dried with Na_2SO_4, and filtered. The filtrate was concentrated, and the residue was purified by FC (EtOAc/hexane = 2/8) to give **3** as a colorless oil (2.2 g, 96.1%). ^{1}H NMR (400 MHz, $CDCl_3$) δ: 7.33–7.26 (m, 2H), 7.17–7.07 (m, 2H), 6.67–6.60 (m, 1H), 5.68–5.64 (m, 1H), 5.18–5.16 (m, 1H), 1.44 (s, 9H). ^{13}C NMR (100 MHz, $CDCl_3$) δ: 154.680, 143.352, 136.208, 134.638, 126.365, 125.351, 113.559, 80.326, 28.381. HRMS (ESI) calcd for $C_{28}H_{32}D_6N_2NaO_4$ [2 M Na] , 495.3106; found, 495.3052.

*2.2.2. tert-Butyl(E)-(4-(2-(6-(2-(2-(2-hydeoxyethoxy)ethoxy)ethoxy) pyridine-3-yl)vinyl)phenyl)(methyl-D3)carbamate (**4**)*

A solution of **3** (1 g, 4.1 mmol), 2-[2-[2-[(5-iodo-2-pyridinyl)oxy] ethoxy]ethoxy]ethanol (1.47 g, 4.1 mmol), potassium carbonate (0.69 g, 5.0 mmol), tetrabutylammonium bromide (1.29 g, 4.0 mmol), and palladium acetate (22 mg, 0.10 mmol) in 15 mL of DMF was deoxygenated by purging with nitrogen for 15 min and then heated at 65 °C for 2 h. The solution was cooled to rt, diluted with 80 mL of ethyl acetate, and washed with brine (20 mL). The organic layer was dried with Na_2SO_4 and filtered. The filtrate was concentrated, and the residue was purified by FC (EtOAc/hexane = 8/2) to give **4** as a white solid (1.27 g, 65.2%). ^{1}H NMR (400 MHz, $CDCl_3$) δ: 168.04 (d, *J = 2.0 Hz*, 1H), 7.85 (s, 1H), 7.65–7.62 (m, 1H), 7.31–7.29 (m, 2H), 7.10–7.08 (m, 2H), 6.82 (s, 2H), 6.67–6.64 (m, 1H), 4.37–4.36 (m, 2H), 3.73 (t, *J = 2.0 Hz*, 2H), 3.59–3.55 (m, 6H), 3.49–3.47 (m, 2H), 1.34 (s, 9H). ^{13}C NMR (100 MHz, $CDCl_3$) δ: 163.244, 154.862, 145.822, 143.353, 135.601, 134.297, 127.538, 126.996, 126.640, 125.644, 124.669, 111.652, 80.635, 72.692, 7.0901, 70.609, 69.950, 65.389, 62.000, 28.555. HRMS (ESI) calcd for $C_{25}H_{31}D_3N_2O_6$ [M H] , 462.2683; found, 462.2703.

*2.2.3. (E)-2-(2-(2-((5-(4-((tert-Butoxycarbonyl)(methyl-D3)amino) styryl-D3)pyridine-2-yl)oxy)ethoxy)ethyl 4-methylbenzenesulfonate (**5**)*

To a solution of **4** (1 g, 2.1 mmol) in 20 mL of DCM at 0 °C were sequentially added 2 mL of Et_3N, TsCl (1.64 g, 8.7 mmol) and 10 mg of DMAP, and the reaction was stirred at 0 °C for 0.5 h and then at rt overnight. The solution was then washed with brine (20 mL), and the organic layer was dried with Na_2SO_4 and filtered. The filtrate was concentrated, and the residue was purified by FC to give **5** as a light-yellow oil (1.24 g, 93.2%). ^{1}H NMR (400 MHz, $CDCl_3$) δ: 8.04 (d, *J = 2.4 Hz*, 1H), 7.81–7.77 (m, 3H), 7.44 (dd, *J = 1.6 Hz*, 2H), 7.11 (dd, *J = 1.6*, 2H), 7.23 (d, *J = 8.8 Hz*, 2H), 6.96 (d, *J = 2.4 Hz*, 2H), 6.79 (d, *J = 8.8 Hz*, 1H), 4.48–4.46 (m, 2H), 4.17–4.15 (m, 2H), 3.83–3.81 (m, 2H), 3.70–3.60 (m, 6H), 2.43 (s, 3H), 1.47 (s, 9H). ^{13}C NMR (100 MHz, $CDCl_3$) δ: 163.240, 154.837, 145.814, 144.953, 143.334, 135.555, 134.268, 133.223, 129.991, 128.165, 127.515, 126.947, 126.621, 125.621, 124.634, 111.611, 80.615, 70.959, 70.813, 69.950, 69.433, 68.910, 65.415, 28.533, 21.811. HRMS (ESI) calcd for $C_{32}H_{37}D_3N_2O_8S$ [M H] , 616.2772; found, 616.2741.

*2.2.4. (E)-2-(2-(2-((5-(4-((tert-Butoxycarbonyl)(methyl-D3)amino) styryl-D3)pyridine-2-yl)oxy)ethoxy)ethoxy)ethyl fluoride (**6**)*

A solution of **5** (0.1 g, 0.16 mmol) and tetrabutylammonium fluoride (0.25 mL, 1.0 M in THF) in 1.5 mL of THF was stirred at 70 °C for 4 h. The reaction mixture was concentrated under vacuum, and the residue was purified by FC to give **6** as a white solid (64 mg, 85.4%). ^{1}H NMR (400 MHz, $CDCl_3$) δ: 8.19 (d, *J = 2.0 Hz*, 1H), 7.81–7.79 (m, 1H), 7.64–7.44 (m, 2H), 7.28–7.23 (m, 2H), 6.98 (d, *J = 2.0 Hz*, 2H), 6.79 (d, *J = 8.4 Hz*, 1H), 4.63 (d, *J = 4.0 Hz*, 1H), 4.53–4.50 (m, 3H), 3.90–3.87 (m, 2H), 3.83–3.72 (m, 6H), 1.48 (s, 9H). ^{13}C NMR (100 MHz, $CDCl_3$) δ: 163.313, 154.877, 145.863, 143.360, 135.549, 134.316, 127.512, 126.946, 126.646, 125.657, 124.698, 111.652, 84.220, 82.540, 80.648, 71.067, 70.947, 70.769, 70.574, 70.017, 65.487, 28.563. ^{19}F NMR (376.5 MHz, $CDCl_3$) δ: -75.461. HRMS (ESI) calcd for $C_{25}H_{30}D_3FN_2O_5$ [M H] , 464.2640; found, 464.2619.

*2.2.5. (E)-2-(2-(2-((5-(4-(Methyl-D3)amino)styryl-D3)pyridine-2-yl-oxy)ethoxy)ethoxy)ethyl fluoride (**7**)*

A solution of **6** (30 mg, 0.06 mmol) and 1 mL of trifluoroacetic acid (TFA) was stirred at rt for 10 min. The reaction mixture was concentrated under vacuum, and the residue was purified by FC to give **7** as a white solid (19 mg, 81.5%). ^{1}H NMR (400 MHz, $CDCl_3$) δ: 8.51 (s, 1H), 8.23 (d, *J = 2.0 Hz*, 1H), 8.01 (dd, *J = 2.4 Hz*, 1H), 7.65 (dd, *J = 1.6 Hz*, 2H), 7.31 (dd, *J = 1.6 Hz*, 2H), 7.15 (d, *J = 3.2 Hz*, 2H), 6.85 (d, *J = 8.4 Hz*, 1H), 4.59 (t, *J = 4.0 Hz*, 1H), 4.47–4.45 (m, 3H), 3.88–3.86 (m, 2H), 3.78–3.86 (m, 2H), 3.78–3.09 (m, 6H). ^{13}C NMR (100 MHz, $CDCl_3$) δ: 162.936, 145.161, 144.406, 135.855, 131.292, 127.962, 127.861, 127.328, 122.888, 116.650, 111.642, 84.219, 82.540, 71.054, 70.954, 70.766, 70.571, 69.975, 65.835. ^{19}F NMR (376.5 MHz, $CDCl_3$) δ: -75.650. HRMS (ESI) calcd for $C_{20}H_{22}D_3FN_2O_3$ [M H] . 364.2116; found, 364.2097.

*2.2.6. (E)-2-(2-(2-((5-(4-((Methyl-D3)amino)styryl-D3)pyridin-2-yl) oxy)ethoxy)ethoxy)ethan-1-ol (**8**)*

A solution of **4** (100 mg, 0.217 mmol) in 0.9 mL of TFA and 0.1 mL of dimethyl sulfide was stirred at rt for 1 h. The reaction mixture was concentrated under vacuum, and the residue was purified by FC (DCM/MeOH = 95/5) to give **8** as a yellowish oil (67 mg, 85.5%). ^{1}H NMR (400 MHz, $CDCl_3$) δ: 8.16 (d, 1H, *J = 2.2 Hz*), 7.78 (dd, 1H, *J = 2.4 Hz*, *J = 8.8 Hz*), 7.36 (d, 2H, *J = 8.4 Hz*), 6.78–6.95 (m, 3H), 6.62 (d, 2H, *J = 8.4 Hz*), 4.51–4.53 (m, 2H), 3.88–3.90 (m, 2H), 3.71–3.77 (m, 6H), 3.63–3.66 (m, 2H). ^{13}C NMR (100 MHz, MeOD) δ: 164.001, 151.292, 145.871, 136.834, 130.280, 129.733, 128.778, 127.641, 120.640, 113.725, 112.198, 73.865, 71.882, 71.580, 70.898, 66.685, 62.390. HRMS (ESI) calcd for $C_{20}H_{24}D_3N_2O_4$ [M H] , 362.2159; found, 362.2196.

*2.2.7. tert-Butyl(E)-(4-(2-(6-(2-(2-(2-chloroethoxy)ethoxy)ethoxy) pyridin-3-yl)vinyl)phenyl)(methyl-D3)carbamate (**9**)*

LiCl (8.3 mg, 0.195 mmol) was added to a solution of **5** (40 mg, 0.065 mmol) in 20 mL of DMF. After stirring at 60 °C for 5 h, the mixture was poured into 50 mL of EtOAc and washed with H_2O (20 mL × 2) as well as brine (20 mL). The organic layer was dried with Na_2SO_4 and filtered. The filtrate was concentrated, and the residue was purified by FC (EtOAc/hexane = 1/1) to give **9** as a white solid (25 mg, 80%). ^{1}H NMR (400 MHz, $CDCl_3$) δ: 8.20 (d, 1H, *J = 2.6 Hz*), 7.80 (dd, 1H, *J = 2.2 Hz*, *J = 8.6 Hz*), 7.45 (d, 2H, *J = 8.4 Hz*), 7.23 (d, 2H, *J = 8.6 Hz*), 6.98 (s, 2H), 6.81 (d, 1H, *J = 8.4 Hz*), 4.50–4.52 (m, 2H), 3.87–3.90 (m, 2H), 3.71–3.79 (m, 6H), 3.63–3.66 (m, 2H), 1.47 (s, 9H). ^{13}C NMR (100 MHz, $CDCl_3$) δ: 163.311, 154.871, 145.866, 143.372, 135.571, 134.320, 127.536, 126.970, 126.655, 125.665, 124.7000, 111.659, 80.653, 71.642, 70.919, 70.039, 65.480, 42.920, 29.910, 28.571. HRMS (ESI) calcd for $C_{25}H_{31}D_3ClN_2O_5$ [M H] , 480.2345; found, 480.2349.

*2.2.8. (E)-4-(2-(6-(2-(2-(2-Chloroethoxy)ethoxy)ethoxy)pyridin-3-yl)vinyl)-N-(methyl-D3)aniline (**10**)*

A solution of **9** (25 mg, 0.052 mmol) in 0.9 mL of TFA and 0.1 mL of dimethyl sulfide was stirred at rt for 1 h. The reaction mixture was concentrated under vacuum, and the residue was purified by FC (DCM/MeOH = 92.5/7.5) to give **10** as s yellowish oil (15 mg, 75.9%). ^{1}H NMR (400 MHz, $CDCl_3$) δ: 8.22 (d, 1H, *J = 2.2 Hz*), 7.83 (dd, 1H, *J = 2.4 Hz*, *J = 8.8 Hz*), 7.47 (d, 2H, *J = 8.4 Hz*), 7.13 (d, 2H, *J = 8.0 Hz*), 6.95 (s, 2H), 6.84 (d, 1H, *J = 8.4 Hz*), 4.51–4.53 (m, 2H), 3.88–3.90 (m, 2H), 3.71–3.77 (m, 6H), 3.63–3.66 (m, 2H). ^{13}C NMR (100 MHz, $CDCl_3$) δ: 163.268, 145.659, 139.971, 135.843, 135.363, 127.999, 126.925, 126.724, 125.190, 120.068, 111.697, 71.604, 70.887, 69.941, 65.768, 42.916. HRMS (ESI) calcd for $C_{20}H_{23}D_3ClN_2O_3$ [M H] , 380.1820; found, 380.1805.

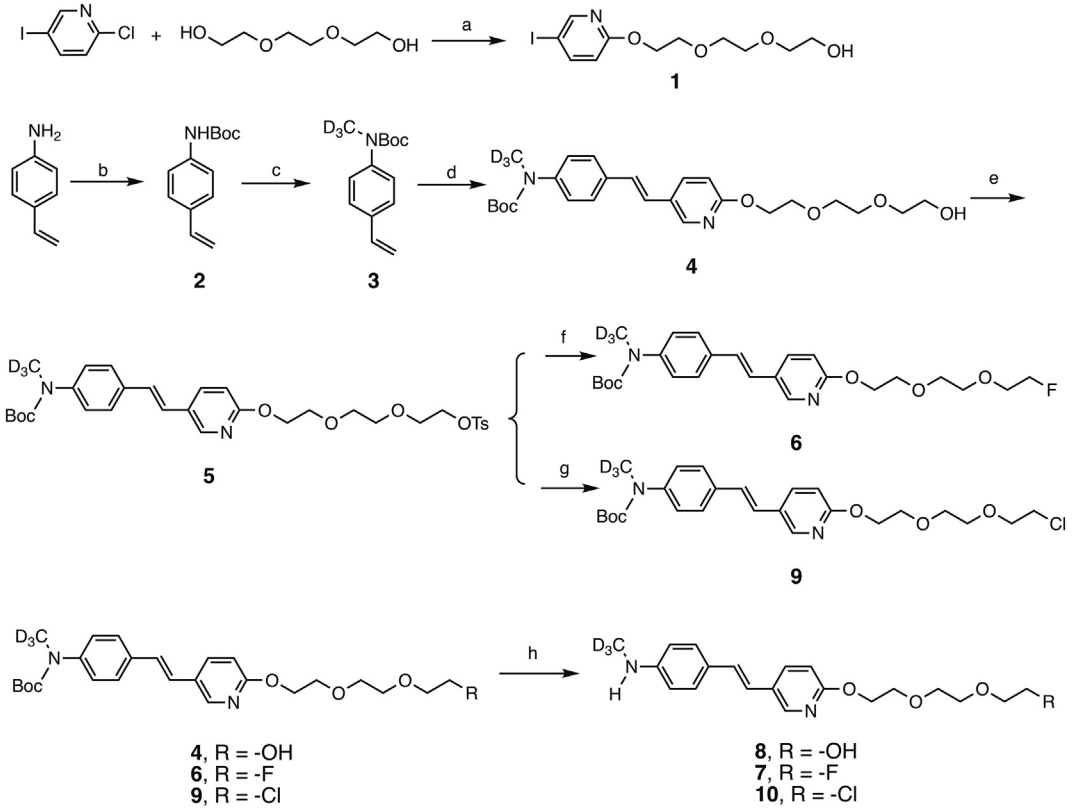

[a]Reagent and conditions: (a) Cs_2CO_3, DMF, 150°C; (b) $(Boc)_2O$, H_2O, 35 °C; (c) NaH, CD_3I, DMF, rt; (d) **1**, TBAB, K_2CO_3, $Pb(Ac)_2$, DMF, 65°C; (e) Et_3N, TsCl, DMAP, DCM, 0°C; (f) TBAF, THF, 70°C; (g) LiCl, DMF, 60°C; (h) TFA, rt.

Scheme 1. Synthesis of deuterated styrylpyridine derivatives **4**–**10**.

2.3. Optimization of the fluorination conditions of O-tosylated compound 5

2.3.1. Fluorination of O-tosylated compound 5 under different temperatures and times

O-Tosylated compound **5** (1 mg, 1.6 μmol) dissolved in 1 mL of DMSO was added into a reaction vial containing the dried K[^{18}F]F/K222 complex (11–37 MBq). The mixture was heated at different temperatures (90, 110, 130 and 150 °C). Aliquots of the mixtures (20 μL) were taken at different time points (5, 10 and 20 min), quenched in ice water and analyzed by HPLC. The radiochemical yield (RCY) of Boc-[^{18}F]D3FSP ([^{18}F]**6**) and the residual amount of unreacted precursor **5** were determined by HPLC.

2.3.2. Fluorination of O-tosylated compound 5 in different solvents

Solutions of *O*-tosylated compound **5** (1 mg, 1.6 μmol) in different solvents (DMSO, DMF or DMA, 1 mL) were mixed with dried K[^{18}F]F/K222 complex (11–37 MBq). The mixtures were heated at 130 °C for 10 min (Scheme 2). Aliquots of the mixtures (20 μL) were periodically taken, quenched in ice water and analyzed by HPLC. The RCY of Boc-[^{18}F]D3FSP ([^{18}F]**6**) was determined by radio-HPLC.

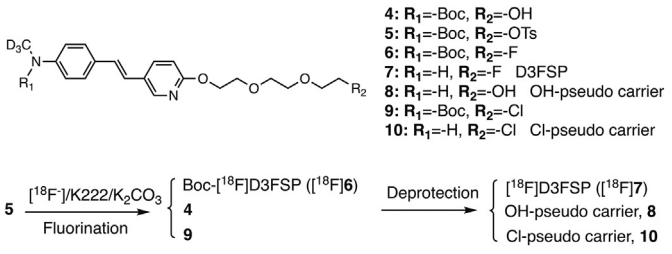

Scheme 2. Radiosynthesis of [^{18}F]D3FSP ([^{18}F]**7**). The byproducts, OH-pseudocarrier (**8**) and Cl-pseudocarrier (**10**), were produced after the radiosynthesis.

2.3.3. Deprotection conditions of Boc-[18F]D3FSP ([18F]6)

To remove the *N*-Boc group of Boc-[^{18}F]D3FSP ([^{18}F]**6**), different acid solutions (3 M HCl, 2 M H_2SO_4 or 1 M TsOH) were added to vials containing solutions of Boc-[^{18}F]D3FSP ([^{18}F]**6**) in DMSO. The mixtures were heated at 100 °C for 5 min (Scheme 2). Aliquots of the mixtures (20 μL) were periodically taken, quenched in ice water and analyzed by HPLC. The remaining amounts of Boc-[^{18}F]D3FSP ([^{18}F]**6**) were determined by radio-HPLC.

2.4. SPE purification of [18F]D3FSP ([18F]7)

The crude product solution was neutralized and diluted with 10 mL of 0.3 M NaOH solution to reach a total volume of 12 mL. The mixture was passed through Sep-Pak® light tC18, Sep-Pak® light tC2, Oasis HLB 3 cc, Sep-Pak® light C8, CHROMAFIX® C18 hydra, CHROMAFIX® C18 or CHROMAFIX® C4 cartridges (pretreated with 10 mL of EtOH followed by 10 mL of H_2O). Then, each cartridge was rinsed with 2 mL of different concentrations of EtOH/H_2O or ACN/H_2O. The eluates were analyzed by HPLC. The appropriate cartridges and optimized eluents were determined based on which offered the lowest amount of residual OH-pseudocarrier (**8**) and the greatest retention of the desired product, [^{18}F]D3FSP ([^{18}F]**7**). To improve the efficiency the SPE purification, the selected cartridges were washed with increasing volumes of EtOH/H_2O and ACN/H_2O. The eluates were then analyzed by HPLC.

Table 1
RCY of Boc-[^{18}F]D3FSP ([^{18}F]**6**) and amounts of chemical impurities under different fluorination temperatures and times using DMSO as the solvent ($n = 3$).

Temp (°C)	Time (min)	RCY of [^{18}F]**6**[a]	Amount of residual precursor, **5** (μg)[b]	Amount of produced Boc-OH-pseudocarrier, **4** (μg)[b]
90	5	47.3 ± 4.2%	404.0 ± 16.9	166.5 ± 46.7
	10	61.3 ± 4.3%	207.6 ± 72.2	293.0 ± 101.3
	20	63.2 ± 6.9%	65.6 ± 44.1	467.1 ± 9.0
110	5	76.2 ± 4.4%	217.5 ± 33.1	294.7 ± 2.9
	10	79.5 ± 4.8%	56.3 ± 11.8	409.8 ± 39.0
	20	71.1 ± 6.3%	0.0 ± 0.0	498.3 ± 31.4
130	5	89.5 ± 2.4%	28.4 ± 18.0	447.8 ± 54.1
	10	89.4 ± 1.7%	0.0 ± 0.0	553.2 ± 20.1
	20	82.7 ± 5.4%	0.0 ± 0.0	507.8 ± 16.9
150	5	85.4 ± 10.1%	0.0 ± 0.0	527.4 ± 32.8
	10	90.3 ± 1.9%	0.0 ± 0.0	504.2 ± 26.5
	20	83.6 ± 12.0%	0.0 ± 0.0	507.6 ± 45.3

[a] RCY of Boc-[^{18}F]D3FSP ([^{18}F]**6**) was determined by HPLC.
[b] Amounts of chemical impurities were calculated based on calibration curves (supplementary Fig. S7).

2.5. RCY, RCP and pseudocarriers in [^{18}F]D3FSP ([^{18}F]**7**) using the optimized radiosynthesis and SPE purification method

The RCY and radiochemical purity (RCP) were measured by an Agilent 1200 series HPLC system equipped with a gamma ray radiodetector (Bioscan) and a UV/Vis detector (Agilent 1200 series). The pseudocarriers remaining in the SPE-purified [^{18}F]D3FSP ([^{18}F]**7**) product were identified by LC/MS, and the amounts were calculated using calibration curves. HPLC chromatograms were acquired using an Agilent Ascentis-C18 column (150 × 4.6 mm) and UV spectroscopic detection at 350 nm with a flow rate of 1 mL/min and the following gradient: 0–2 min: 95% A, 5% B; 2–5 min: 95%–30% A, 5%–70% B; 5–10 min: 30%–1% A, 70%–99% B; 10–15 min: 1%–95% A, 99%–5% B; and 15–20 min: 95% A, 5% B. Mobile phase A was water with 10 mM ammonium formate buffer (AFB) and mobile phase B was ACN. LC/MS data were recorded in ESI positive ion mode on an Agilent G3250AA LC/MSD TOF system (Santa Clara, CA). An Agilent Poroshell 120 EC-C18 column (50 × 3.0 mm) with UV spectroscopic detection at 350 nm were used with a flow rate of 0.4 mL/min and the same gradient conditions as described above for the HPLC separation.

2.6. In vitro binding assay of [^{18}F]D3FSP ([^{18}F]**7**)

Postmortem AD brain tissues were homogenized and frozen at −80 °C until being used in the binding assay. A competitive binding assay was performed in PBS (pH = 7.4, containing 0.1% BSA) using [^{18}F]D3FSP ([^{18}F]**7**) and 10^{-10}–10^{-5} M cold competing drugs ("cold" AV-45, D3FSP (**7**), OH-pseudocarrier (**8**), and Cl-pseudocarrier (**10**)). Nonspecific binding was defined with 5.5 μM IMPY. After incubation at 37 °C for 2 h, the bound and free radioactive material were separated by vacuum filtration through GF/B filter paper using a Brandel M-24R cell harvester. The filter papers were washed twice with cold Tris-HCl buffer (50 mM, pH = 7.4), and the radioactivity on each filter paper was counted with a gamma counter (Wizard^2, Perkin-Elmer) with 50% efficiency. Competition experiments were analyzed using a nonlinear regression algorithm, and the Cheng-Prusoff equation was used to obtain the inhibition constant (K_i) values.

Table 2
RCY of Boc-[^{18}F]D3FSP ([^{18}F]**6**) in different solvents ($n = 3$).

Solvent[a]	RCY of [^{18}F]**6**[b]
DMSO	73.9 ± 14.3%
DMF	44.6 ± 10.8%
DMA	15.8 ± 2.8%

[a] DMSO = Dimethyl sulfoxide; DMF = *N,N*-Dimethylformamide; DMA = *N,N*-Dimethylacetamide.
[b] RCY of Boc-[^{18}F]D3FSP ([^{18}F]**6**) was determined by HPLC (Supplementary Fig. S1).

Table 3
Amount of Boc-[^{18}F]D3FSP ([^{18}F]**6**) remaining in the reaction mixture when using different acids for the deprotection for 5 min ($n = 3$) (data derived from HPLC, see Fig. S2).

Acid	[^{18}F]**6**
3 M HCl	0%
2 M H_2SO_4	0%
1 M TsOH	0%

3. Results and discussion

3.1. Chemistry

Deuterated styrylpyridine derivatives **4**–**10** were successfully synthesized by the reactions described in Scheme 1. Iodomethane-D3 was reacted with *tert*-butyl (4-vinylphenyl)carbamate (**2**) to give deuterated compound **3** in 96% yield. Compound **3** was coupled with 2-(2-(2-((5-iodopyridin-2-yl)oxy)ethoxy)ethoxy)ethan-1-ol (**1**) to yield **4** in 65% yield. *O*-Tosylated compound **5** was assembled by the reaction of compound **4** and *m*-toluenesulfonyl chloride in 93% yield and was converted to fluoride compound **6** and chloride compound **9** with tetrabutylammonium fluoride and lithium chloride in 85% and 80% yields, respectively. Subsequently, the *tert*-butyl protecting groups of **4**, **6** and **9** were removed by TFA to give **8**, **7** and **10** in 86%, 82% and 76% yields, respectively. The major impurities in the intermediate, Boc-[^{18}F]D3FSP ([^{18}F]**6**), were *N*-Boc protected **4** and **9**; the final product, [^{18}F]D3FSP ([^{18}F]**7**), contained OH-pseudocarrier **8** and Cl-pseudocarrier **10**. Authentic samples of these impurities were prepared, and their LC/MS and HPLC profiles were determined to facilitate chemical analysis.

Initially, *N*-Boc protected *O*-tosylate precursor **5** was prepared for the fluorination reaction. A preliminary fluorination reaction with [^{18}F]F$^-$ was carried out. The intermediate, Boc-[^{18}F]D3FSP ([^{18}F]**6**), and the final product, [^{18}F]D3FSP ([^{18}F]**7**), contained small amounts (20 and 2 μg per batch) of chloride derivatives **9** and **10**. The compounds were identified by comparison with authentic samples of **9** and **10** that had been prepared separately (using both LC/MS and HPLC profiles). It was suspected that the chloride impurities might be produced during the initial fluorination and HCl deprotection reactions. However, further studies using sulfuric acid and toluenesulfonic acid, which lack chloride ions, for deprotection of the *N*-Boc group afforded similar amounts of the chloride impurity (1–2 μg of Cl-pseudocarrier **10**), suggesting that HCl was not the source of Cl-pseudocarrier **10**. To rule out the possibility that *N*-Boc protected *O*-tosylated precursor **5** was not the source of Cl-pseudocarrier **10**, **5** was further purified by HPLC to remove any impurities. When repurified **5** was labeled using the same fluorination and deprotection strategy with HCl, the same amount of Cl-pseudocarrier (1–2 μg of **10**) was observed. Thus, by a process of elimination, the most likely source of Cl-pseudocarrier **10** was the [^{18}F]F$^-$ solution, which was obtained from the PET/cyclotron at the University of Pennsylvania. Fortunately, the amount of Cl-pseudocarrier **10** in the final product ([^{18}F]D3FSP ([^{18}F]**7**)) was very small (2 ± 1 μg per batch). One may also consider that a chloride containment might be present in many other ^{18}F tracers similarly produced from other *O*-tosylated precursors.

One of the most important and widely used ^{18}F labeling reactions is the labeling of mannose 2-*O*-triflate for the synthesis of [^{18}F]FDG (Juelich method) [51]. Similarly, it was reported that a chloride impurity, ClDG, was one of the impurities in final doses of [^{18}F]FDG [42,52,53]. It was suggested in that report that "it is unlikely that the presence of small quantities of ClDG found in typical FDG preparations (ca. 100 μg) would have adverse pharmacological or toxicological consequence" [52].

Table 4
Removal of OH-pseudocarrier **8** and retention of [^{18}F]D3FSP ([^{18}F]**7**) on the cartridge when the SPE cartridge was washed with 2 mL of increasing concentration of EtOH/H_2O and ACN/H_2O. The appropriate ranges of ACN/H_2O and EtOH/H_2O concentrations were defined as those that maximized the removal of OH-pseudocarrier **8** and the retention of [^{18}F]D3FSP ([^{18}F]**7**) on the cartridge.

SPE cartridge	2 mL of ACN/H_2O as the eluent			2 mL of EtOH/H_2O as the eluent		
	Concentration of ACN/H_2O	Removal of **8**	Retention of [^{18}F]**7**	Concentration of EtOH/H_2O	Removal of **8**	Retention of [^{18}F]**7**
SPE c1	30–40%	0–91.0%	97.3–91.2%	30–40%	1.4–98.7%	4.1–97.3%
SPE c2	20–30%	71.8–98.3%	89.2–44.2%	30–40%	77.0–88.8%	66.3–46.3%
SPE c3	30–40%	25.5–98.7%	92.7–83.6%	70–80%	6.9–97.2%	97.0–35.4%
SPE c4	20–30%	65.9–96.6%	70.8–27.4%	20–30%	40.9–92.1%	79.3–23.2%
SPE c5	50–60%	81.4–95.7%	32.1–6.6%	50–60%	66.4–88.4%	40.3–14.1%
SPE c6	40–50%	42.3–98.0%	10.5–0%	40–50%	49.2–91.0%	64.1–13.6%
SPE c7	30–40%	5.3–95.9%	93.7–55.0%	30–40%	4.8–87.0%	96.3–31.2%

Note: SPE c1: Sep-Pak® light tC18 cartridge; SPE c2: Sep-Pak® light tC2 cartridge; SPE c3: Oasis HLB 3 cc cartridge; SPE c4: Sep-Pak® light C8 cartridge; SPE c5: CHROMAFIX® C18 hydra cartridge; SPE c6: CHROMAFIX® C18 cartridge; SPE c7: CHROMAFIX® C4 cartridge.

3.2. Fluorination reaction conditions of *O*-tosylated compound **5**

A series of studies were carried out to determine the optimal fluorination conditions. The radiochemical yield (RCY) of Boc-[^{18}F]D3FSP ([^{18}F]**6**) and the amounts of residual *O*-tosylated precursor **5** and produced Boc-OH-pseudocarrier **4** generated using different temperatures and times were determined (Table 1). One objective of this study was to maximize the RCY and to minimize the residual *O*-tosylated precursor (residual precursor may complicate the solid-phase extraction step). As shown in Table 1, the RCY of Boc-[^{18}F]D3FSP ([^{18}F]**6**) improved with increasing reaction temperature (61% at 90 °C, 79% at 110 °C, 89% at 130 °C and 90% at 150 °C in DMSO for 10 min). When fluorination was carried out at 110 °C (20 min), 130 °C (10 min, 20 min) and 150 °C (5 min, 10 min, and 20 min), the precursor was completely consumed, and comparable RCYs of Boc-[^{18}F]D3FSP ([^{18}F]**6**) were observed.

The RCY of Boc-[^{18}F]D3FSP ([^{18}F]**6**) was also dependent on the solvent. As shown in Table 2, the RCY was 74% in DMSO, which was higher than those obtained in DMF and DMA (45% and 16%, respectively). Therefore, DMSO was the solvent of choice. The optimized conditions for fluorination were heating at 130 °C for 10 min, an under these conditions *O*-tosylated precursor **5** was completely consumed.

3.3. Deprotection conditions of Boc-[^{18}F]D3FSP ([^{18}F]**6**)

The second step in the synthesis, the *N*-Boc deprotection reaction of Boc-[^{18}F]D3FSP ([^{18}F]**6**), was carried out at 100 °C for 5 min using three different acids, 3 M HCl, 2 M H_2SO_4 or 1 M TsOH, to give [^{18}F]D3FSP ([^{18}F]**7**). As shown in Table 3, all three acids showed comparable high efficiencies (100% deprotection in 5 min). The reason for testing different acids for removing the *N*-Boc protecting group was the possible introduction of Cl-pseudocarrier **10** when hydrochloric acid was used for the deprotection (the introduction of Cl- ions into the solution might have led to production of the undesired Cl-derivative). However, all three acids effectively catalyzed the deprotection without introducing additional undesired Cl-pseudocarrier **10** (Supplementary Figs. S2, S3 and S4). It is likely that the Cl- ions were introduced by the initial [^{18}F] fluoride solution. Considering the ease of use, HCl solution was used for the deprotection *via* hydrolysis.

3.4. SPE purification of [^{18}F]D3FSP ([^{18}F]**7**)

After deprotection of the *N*-Boc group, the crude reaction mixture was purified using SPE. Based on the UV-HPLC chromatogram of the crude product, three major chemical impurities were expected (Fig. 5B). They are OH-pseudocarrier **8** (530 ± 170 μg), D3FSP (**7**, 2 ± 1 μg) and Cl-pseudocarrier **10** (2 ± 1 μg). The goal of the SPE method was to reduce the amount of chemical impurities and to minimize the loss of [^{18}F]D3FSP ([^{18}F]**7**) as much as possible. Different concentrations and volumes of EtOH/H_2O and ACN/H_2O were tested in conjunction with seven different reversed-phase SPE cartridges (SPE c1: Sep-Pak® light tC18 cartridge; SPE c2: Sep-Pak® light tC2 cartridge; SPE c3: Oasis HLB 3 cc cartridge; SPE c4: Sep-Pak® light C8 cartridge; SPE c5: CHROMAFIX® C18 hydra cartridge; SPE c6: CHROMAFIX® C18 cartridge; and SPE c7: CHROMAFIX® C4 cartridge).

First, 2 mL of different concentrations of EtOH/H_2O and ACN/H_2O were used to wash the SPE cartridges (to maximize the removal of OH-pseudocarrier **8** and the retention of [^{18}F]D3FSP ([^{18}F]**7**) on the cartridge). The appropriate ranges of ACN/H_2O concentrations when using a Sep-Pak® light tC18 cartridge, a Sep-Pak® light tC2 cartridge and an Oasis HLB 3 cc cartridge were 30–40% ACN/H_2O, 20–30% ACN/H_2O and 30–40% ACN/H_2O, respectively, and these solvent systems resulted in >95% removal of OH-pseudocarrier **8** and > 80% retention of [^{18}F]D3FSP ([^{18}F]**7**) on the cartridge, as shown in Table 4 (Supplementary Fig. S5).

To enhance the efficiency of the SPE purification, three types of cartridges (Sep-Pak® light, tC2 and Oasis 3 cc cartridges) were tested in detail. They were washed with increasing volumes of the combinations of solvents listed in Table 5. After HPLC analysis of the eluate, the optimized SPE purification conditions were selected based on maximizing the retention of [^{18}F]D3FSP ([^{18}F]**7**) and removing undesired OH-pseudocarrier **8**. As shown in Table 5, >95% of OH-pseudocarrier **8** was removed, and >80% of [^{18}F]D3FSP ([^{18}F]**7**) was retained when the tC18 cartridge was washed with 6 mL of 30% ACN/H_2O, 6 mL of 35% ACN/H_2O and 2 mL of 40% ACN/H_2O; the tC2 cartridge was washed with 6 mL of 25% ACN/H_2O; or the Oasis 3 cc cartridge was washed with 8 mL 35% of ACN/H_2O. Among these SPE purification conditions, washing the tC18 cartridge with 6 mL of 30% ACN/H_2O was selected as the most efficient SPE purification conditions, as 98.0 ± 0.8% of the OH-

Table 5
Second optimized SPE purification using three different cartridges under different combination of conditions resulted in the removal of >95% of OH-pseudocarrier **8** and the retention of >80% of [^{18}F]D3FSP ([^{18}F]**7**).

SPE cartridge	Eluent	Removal of **8**	Retention of [^{18}F]**7**
Sep-Pak® light tC18 cartridge	6 mL 30% ACN/H_2O	98.0 ± 0.8%	92.8 ± 0.1%
	6 mL 35% ACN/H_2O	97.2 ± 0.1%	91.9 ± 1.7%
	2 mL 40% ACN/H_2O	96.5 ± 2.4%	87.4 ± 3.5%
Sep-Pak® light tC2 cartridge	6 mL 25% ACN/H_2O	97.9 ± 0.2%	85.8 ± 3.1%
Oasis HLB 3 cc cartridge	8 mL 35% ACN/H_2O	98.5 ± 0.0%	82.3 ± 5.2%

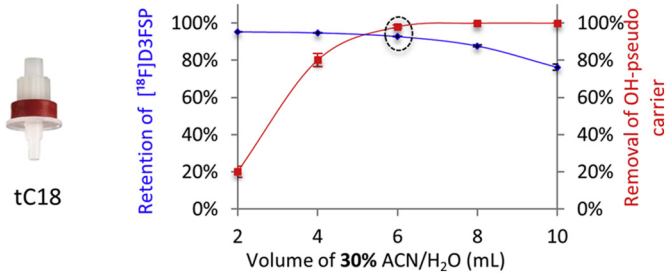

Fig. 4. Removal of OH-pseudocarrier **8** (red line) and retention of [^{18}F]D3FSP ([^{18}F]**7**) (blue line) when the Sep-Pak® light tC18 cartridge was washed with increasing volumes of 30% ACN/H_2O. Using the optimal conditions, as indicated by the dotted circle, 98.0 ± 0.8% of OH-pseudocarrier **8** was removed, while 92.8 ± 0.1% of [^{18}F]D3FSP ([^{18}F]**7**) was retained on the cartridge. When the Sep-Pak® light tC18 cartridge was washed with 6 mL of 30% ACN/H_2O, it provided the best result in terms of maximizing the retention of [^{18}F]D3FSP ([^{18}F]**7**) and removing undesired OH-pseudocarrier **8**. (For interpretation of the references to colour in this figure legend, the reader is referred to the web version of this article.)

pseudocarrier, **8**, was removed and 92.8 ± 0.1% of [^{18}F]D3FSP ([^{18}F]**7**) was retained on the cartridge (Supplementary Fig. S6).

Finally, the optimal purification of the crude reaction mixture of [^{18}F]D3FSP ([^{18}F]**7**) could be achieved by loading the mixture onto a Sep-Pak® light tC18 cartridge (pretreated with 10 mL of EtOH and 10 mL of H_2O). The cartridge was rinsed with 6 mL of 30% ACN to elute unreacted [^{18}F]F^- and most of the OH-pseudocarrier, **8**, and then the cartridge was washed with 10 mL of H_2O and 10 mL of 10% EtOH/H_2O to remove the residual ACN on the cartridge (see Fig. 4, the black dotted circle). The desired product, [^{18}F]D3FSP ([^{18}F]**7**), was obtained by rinsing the cartridge with 2 mL of 50% EtOH/saline into a vial containing 8 mL of normal saline for injection.

*3.5. RCY, RCP and pseudocarriers in [^{18}F]D3FSP ([^{18}F]**7**) using the optimized radiosynthesis and SPE purification method*

The optimized preparation of [^{18}F]D3FSP ([^{18}F]**7**) was implemented in the following sequence. **(1)** The [^{18}F] fluoride (37 to 370 MBq) was trapped on a Sep-Pak® light QMA cartridge (preactivated with 10 mL of 0.5 N $NaHCO_3$ and 10 mL of H_2O) and eluted with 1.1 mL of the eluent (K222 (11 mg)/K_2CO_3 (2 mg) in 0.93 mL of ACN and 0.17 mL of H_2O) into a reaction vial. The mixture was concentrated at 100 °C under a stream of argon and azeotropically dried twice with the addition of 1 mL of anhydrous ACN. **(2)** The fluorination was initiated by adding 1 mg of the precursor, **5**, dissolved in 1 mL of DMSO to the activated K[^{18}F]F/K222 complex. The reaction mixture was heated for 10 min at 130 °C. The reaction vial was cooled for 1 min, and then 1 mL of 3 M HCl solution was added to remove the *N*-Boc group. The mixture was heated at 100 °C for 5 min. After cooling to rt, the reaction mixture was neutralized and diluted with 10 mL of 0.3 M NaOH solution. **(3)** The SPE purification was carried out as follows: the reaction mixture was loaded onto a Sep-Pak® light tC18 cartridge (pretreated with 10 mL of EtOH and 10 mL of H_2O). The cartridge was rinsed with 6 mL of 30% ACN to elute unreacted [^{18}F] fluoride and most of OH-pseudocarrier **8** and then with 10 mL of H_2O and 10 mL of 10% EtOH/H_2O to flush out residual ACN from the cartridge. **(4)** The final product, D3-[^{18}F]FSP ([^{18}F]**7**), was eluted with 2 mL of 50% EtOH/saline into a vial containing 8 mL of normal saline for injection. The purity of the SPE-purified [^{18}F]D3FSP ([^{18}F]**7**) for injection was analyzed by HPLC (Fig. 5).

Using this method, the RCY of [^{18}F]D3FSP ([^{18}F]**7**) was 44.4 ± 5.7% (decay corrected, $n = 10$) with RCP >95% in 50 min. The labeling reaction was carried out at a radioactivity level of 18–444 MBq. The HPLC chromatograms of unpurified [^{18}F]D3FSP ([^{18}F]**7**) and SPE-purified [^{18}F]D3FSP ([^{18}F]**7**) are shown in Fig. 5. There were 2 ± 1 μg of "cold" carrier D3FSP (**7**) and 19 ± 5 μg of OH-pseudocarrier **8** (the quantity of each was determined using calibration curves, see Supplementary Fig. S7). The total mass in the 10 mL of SPE-purified [^{18}F]D3FSP ([^{18}F]**7**) product was 21 ± 5 μg (per batch, n = 10), which is below the total mass of chemical (50 μg) as indicated in the package insert of [^{18}F]AV-45 (florbetapir f 18, Amyvid).

In the future, clinical preparations of [^{18}F]D3FSP ([^{18}F]**7**) will be prepared by an automatic synthesizer at a higher radioactivity level (>3.7 GBq). There will be multiple clinical doses (the recommended dose for Amyvid is 370 MBq) prepared in one run, and it is likely that single doses will contain only a fraction of the 21 ± 5 μg measured mass in one batch of preparation. The chemical mass is unlikely to interfere with Aβ plaque binding in the brain after iv injection. Similar to the commercial production of [^{18}F]FDG, the whole sequences of fluorination and SPE purification of [^{18}F]D3FSP ([^{18}F]**7**) as described above will be easily translated to automation in a hot cell under GMP production conditions. The step established in this paper for the preparation of [^{18}F]D3FSP ([^{18}F]**7**) is suitable for implementation by regional radiopharmacies, which will facilitate widespread clinical application in a large patient population in China or in other locations around the world.

*3.6. In vitro binding assay of D3-[^{18}F]FSP ([^{18}F]**7**)*

An *in vitro* binding assay was used to measure the binding affinities of [^{18}F]D3FSP ([^{18}F]**7**) and the pseudocarriers using postmortem AD brain homogenates. The inhibition constants (K_i, nM) of drugs that competitively inhibit the binding of [^{18}F]D3FSP ([^{18}F]**7**) to Aβ plaques are shown in Table 6. D3FSP, **7**, displayed an excellent and comparable binding affinity to that of AV-45 for Aβ plaques. OH-pseudocarrier **8**, which remained in the SPE-purified [^{18}F]D3FSP ([^{18}F]**7**) product, and Cl-pseudocarrier **10** showed slightly lower binding affinities for Aβ plaques than AV-45 and D3FSP (**7**). The presence of OH-pseudocarrier **8** was known, but the small amount of Cl-pseudocarrier **10** in the fluorination reaction is not well established. Limiting the total chemical mass in a single dose (<50 μg) for PET imaging studies is achievable. The binding data reported in Table 6 also support the contention that the chemical impurities will not interfere with the binding to Aβ aggregates in AD brain.

Preliminary studies in humans (Dr. Dean Wong, Johns Hopkins University, unpublished data, IND #137713) suggested that there were no significant differences in the *in vivo* metabolic *N*-demethylation of [^{18}F]D3FSP ([^{18}F]**7**) and [^{18}F]AV-45. However, [^{18}F]D3FSP ([^{18}F]**7**) displayed facile binding to Aβ plaques in AD patients similar to what is observed with [^{18}F]AV-45 in the same AD patient, and the pharmacokinetic characteristics of the drugs were comparable [54]. [^{18}F]D3FSP ([^{18}F]**7**) appears to be a promising PET imaging agent for mapping Aβ plaques in the brain. The originally hypothesized mechanism for improving Aβ plaque imaging based on deuterium substitution of hydrogens on the *N*-methyl group to slow *in vivo* metabolism might not be realized. In the case of this deuterated *N*-methyl group, replacing hydrogen with deuterium offers no advantage. Although improving the pharmacokinetic properties by deuteration for drug development has led to a number of successes, this strategy is unlikely to be universally applicable. Future applications of deuteration approaches require careful consideration of the *in vivo* kinetics and metabolism. However, preliminary results suggested that [^{18}F]D3FSP ([^{18}F]**7**) might serve as a useful Aβ plaque imaging agent with comparable *in vivo* targeting properties to those of [^{18}F]AV-45 (florbetapir f18, Amyvid).

Since there are already three FDA-approved PET imaging agents (Fig. 1) for imaging Aβ plaques, the obvious question of why another me-too imaging agent is needed remains a relevant concern. A simple answer is that there is no commercially available Aβ plaque imaging agent in China. There are estimated to be over ten million AD patients in China, and there is an urgent unmet clinical need for using PET Aβ plaque imaging as a diagnostic tool. The population in China is aging rapidly, and the potential market for the diagnosis of patients suspected of having AD is larger than the markets in the U.S. and Europe combined. The commercial development of Aβ plaque-targeting imaging agents to

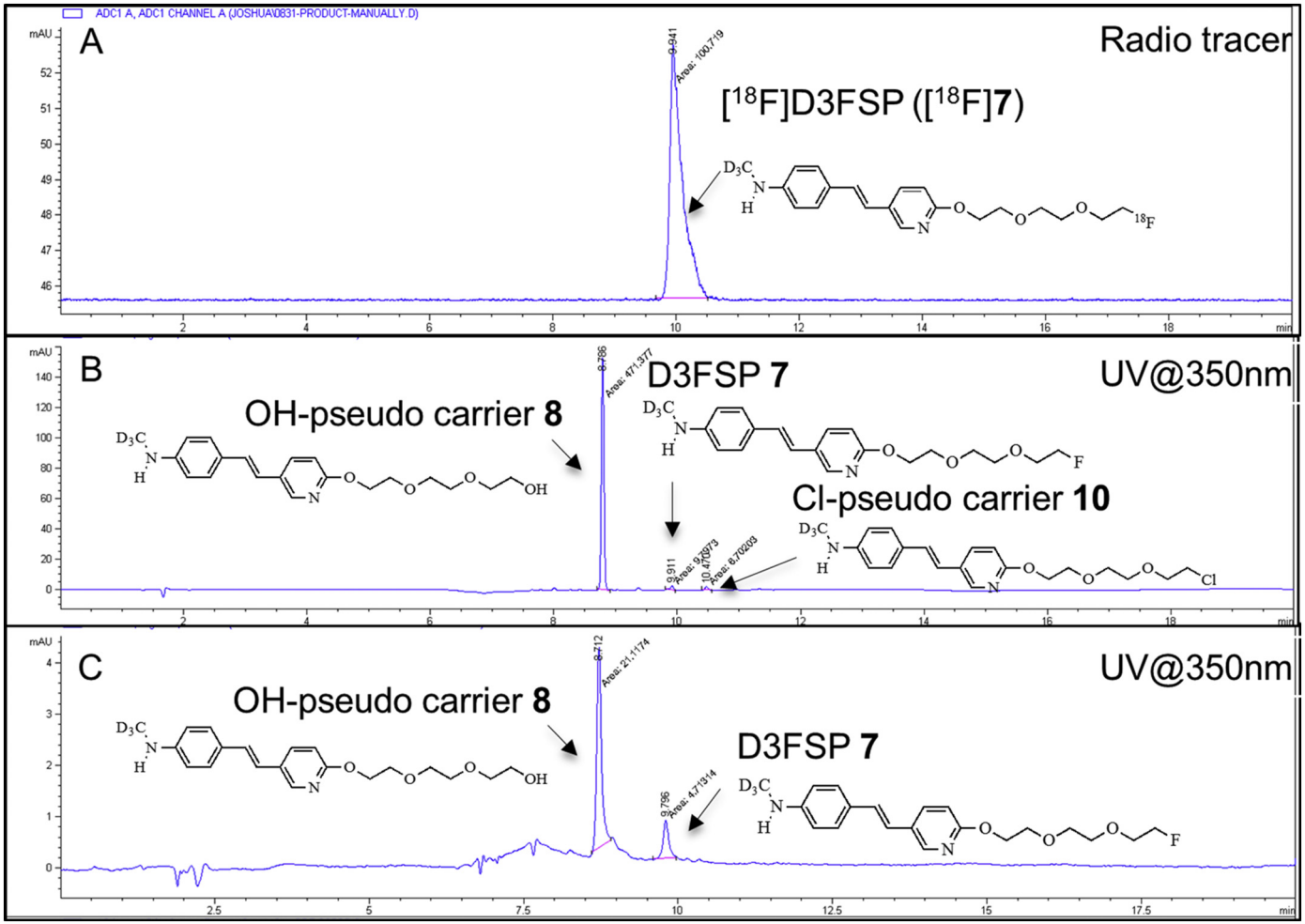

Fig. 5. HPLC profiles of (A) [^{18}F]D3FSP ([^{18}F]**7**) with radio detection, (B) unpurified [^{18}F]D3FSP ([^{18}F]**7**) with UV detection @ 350 nm and (C) SPE-purified [^{18}F]D3FSP ([^{18}F]**7**) with UV detection @ 350 nm. Three main chemical impurities remained in the crude product, including 530 ± 170 μg of OH-pseudocarrier **8**, 2 ± 1 μg of D3FSP **7**, and 2 ± 1 μg of Cl-pseudocarrier **10**. Using SPE purification, the majority of the Cl-pseudocarrier, **10**, was removed, and the amount of residual chemical impurities was reduced to 21 ± 5 μg in the final 10-mL dose of [^{18}F]D3FSP ([^{18}F]**7**).

Table 6
Inhibition constants (K_i values) of drugs competitively inhibiting the binding of [^{18}F]D3FSP ([^{18}F]**7**) to Aβ aggregates in AD brain homogenates ($n = 3$).

Drug	K_i (nM)
AV-45	8.6 ± 0.5
D3FSP, **7**	9.8 ± 0.5
OH-pseudocarrier, **8**	19.5 ± 0.5
Cl-pseudocarrier, **10**	18.6 ± 3.9

serve patients in China is in great demand. Although there are anecdotal reports of human studies performed in local Chinese hospitals as part of research studies by individual neurologists, there is no widespread use of Aβ plaque imaging for facilitating AD diagnosis. The logistics of setting up regional radiopharmacies and registering this new product in China are exceedingly challenging. However, as it stands, without these efforts, there will be no routine clinical studies using PET Aβ plaque imaging available for millions of Chinese patients requiring these tests. Developing [^{18}F]D3FSP ([^{18}F]**7**) as a new Aβ plaque imaging agent for the Chinese market might bypass thorny patent issues, alleviate the unmet clinical need and serve a large number of patients suspected of having AD in China. This is only a small step in meeting the medical needs in a country with a massive population, but it is a worthy effort.

4. Conclusion

In summary, the radiosynthesis and purification of [^{18}F]D3FSP ([^{18}F]**7**) were optimized. Applying this improved method, a Sep-Pak® light tC18 cartridge was rinsed with 6 mL of 30% ACN to eliminate unreacted [^{18}F] fluoride and most of OH-pseudocarrier **8**. The final product, [^{18}F]D3FSP ([^{18}F]**7**), was eluted with 2 mL of 50% EtOH/saline. The desired product [^{18}F]D3FSP ([^{18}F]**7**) was obtained in a good radiochemical yield and purity (RCY was 44.4 ± 5.7%, decay corrected; RCP was >95%) in 50 min, instead of the 105 min required for HPLC purification [55]. The product contains a very low content of pseudocarriers (21.7 ± 5.5 μg per batch), and it will be suitable for human use. This new simplified method might ease the burden of daily routine preparation under GMP manufacturing for clinical applications and facilitate the diagnosis of Alzheimer's disease.

Acknowledgements

This work was supported in part by Five Eleven Pharma Inc., Philadelphia, PA 19104, USA.

Appendix A. Supplementary data

Supplementary data to this article can be found online at https://doi.org/10.1016/j.nucmedbio.2019.05.002.

References

[1] Gilbert BJ. The role of amyloid beta in the pathogenesis of Alzheimer's disease. J Clin Pathol 2013;66:362–6.
[2] Awasthi M, Singh S, Pandey VP, Dwivedi UN. Alzheimer's disease: an overview of amyloid beta dependent pathogenesis and its therapeutic implications along with in silico approaches emphasizing the role of natural products. J Neurol Sci 2016;361:256–71.
[3] Blennow K, Zetterberg H. Biomarkers for Alzheimer's disease: current status and prospects for the future. J Intern Med 2018;284:643–63.
[4] Thal DR, Rüb U, Orantes M, Braak H. Phases of Aβ-deposition in the human brain and its relevance for the development of AD. Neurology 2002;58:1791–800.
[5] Selkoe DJ, Hardy J. The amyloid hypothesis of Alzheimer's disease at 25 years. EMBO Mol Med 2016;8:595–608.
[6] Ballaed C, Gauthier S, Corbett A, Brayne C, Aarsland D, Jones E. Alzheimer's disease. Lancet 2011;377:1019–31.
[7] Nordberg A, Rinne JO, Kadir A, Langstrom B. The use of PET in Alzheimer disease. Nat Rev Neurol 2010;6:78–87.
[8] Herholz K, Carter SF, Jones M. Positron emission tomography imaging in dementia. Br J Radiol 2007;80 Spec No 2:S160–7.
[9] Drzezga A. Amyloid-plaque imaging in early and differential diagnosis of dementia. Ann Nucl Med 2010(2):55–123.
[10] Berti V, Osorio RS, Mosconi L, Li Y, De Santi S, de Leon MJ. Early detection of Alzheimer's disease with PET imaging. Neurodegener Dis 2010;7:131–5.
[11] Bao W, Jia H, Finnema S, Cai Z, Carson RE, Huang YH. PET imaging for early detection of Alzheimer's disease: from pathologic to physiologic biomarkers. PET Clin 2017;12:329–50.
[12] Jack Jr CR, Bennett DA, Blennow K, Carrillo MC, Dunn B, Haeberlein SB, et al. NIA-AA Research Framework: toward a biological definition of Alzheimer's disease. Alzheimers Dement 2018;14:535–62.
[13] Cummings J. The National Institute on Aging-Alzheimer's Association Framework on Alzheimer's disease: application to clinical trials. Alzheimers Dement 2019;15:172–8.
[14] Mallik A, Drzezga A, Minoshima S. Clinical amyloid imaging. Semin Nucl Med 2017;47:31–43.
[15] Khachaturian AS, Hayden KM, Mielke MM, Tang Y, Lutz MW, Gustafson DR, et al. Future prospects and challenges for Alzheimer's disease drug development in the era of the NIA-AA Research Framework. Alzheimers Dement 2018;14:532–4.
[16] Golde TE, DeKosky ST, Galasko D. Alzheimer's disease: the right drug, the right time. Science 2018;362:1250–1.
[17] Klunk WE, Engler H, Nordberg A, Wang Y, Blomqvist G, Holt DP, et al. Imaging brain amyloid in Alzheimer's disease with Pittsburgh Compound-B. Ann Neurol 2004;55:306–19.
[18] Rowe C, Ackerman U, Browne W, Mulligan R, Pike K, O'Keefe G, et al. Imaging of amyloid beta in Alzheimer's disease with (18)F-BAY94-9172, a novel PET tracer: proof of mechanism. Lancet Neurol 2008;7:129–35.
[19] Thal DR, Beach TG, Zanette M, Heurling K, Chakrabarty A, Ismail A, et al. [(18)F] flutemetamol amyloid positron emission tomography in preclinical and symptomatic Alzheimer's disease: specific detection of advanced phases of amyloid-beta pathology. Alzheimers Dement 2015;11:975–85.
[20] Koole M, Lewis D, Buckley C, Nelissen N, Vandenbulcke M, Brooks D, et al. Whole-body biodistribution and radiation dosimetry of 18F-GE067: a radioligand for in vivo brain amyloid imaging. J Nucl Med 2009;50:818–22.
[21] Rowe CC, Jones G, Dore V, Pejoska S, Margison L, Mulligan RS, et al. Standardized expression of 18F-NAV4694 and 11C-PiB beta-amyloid PET results with the centiloid scale. J Nucl Med 2016;57:1233–7.
[22] Oh SJ, Kim MH, Han SJ, Kang KJ, Ko IO, Kim Y, et al. Preliminary PET study of 18F-FC119S in normal and Alzheimer's disease models. Mol Pharm 2017;14:3114–20.
[23] Byun BH, Kim BI, Park SY, Ko IO, Lee KC, Kim KM, et al. Head-to-head comparison of 11C-PiB and 18F-FC119S for Abeta imaging in healthy subjects, mild cognitive impairment patients, and Alzheimer's disease patients. Medicine (Baltimore) 2017;e6441:96.
[24] Wong D, Rosenberg P, Zhou Y, Kumar A, Raymont V, Ravert H, et al. In vivo imaging of amyloid deposition in Alzheimer disease using the radioligand 18F-AV-45 (Flobetapir F 18). J Nucl Med 2010;51:913–20.
[25] Yang L, Rieves D, Ganley C. Brain amyloid imaging—FDA approval of florbetapir F18 injection. N Engl J Med 2012;367:885–7.
[26] Camus V, Payoux P, Barre L, Desgranges B, Voisin T, Tauber C, et al. Using PET with (18)F-AV-45 (florbetapir) to quantify brain amyloid load in a clinical environment. Eur J Nucl Med Mol Imaging 2012;39:11.
[27] Kung H, Choi S, Qu W, Zhang W, Skovronsky D. (18)F stilbenes and styrylpyridines for PET imaging of Abeta plaques in Alzheimer's disease: a miniperspective. J Med Chem 2009;53:933–41.
[28] Kung H. The β-amyloid hypothesis in Alzheimer's disease: seeing is believing. ACS Med Chem Lett 2012;3:265–7.
[29] Choi S, Golding G, Zhuang Z, Zhang W, Lim N, Hefti F, et al. Preclinical properties of 18F-AV-45: a PET agent for Aβ plaques in the brain. J Nucl Med 2009;50:1887–94.
[30] Yin W, Zhou X, Qiao J, Zhu L. Study the pharmacokinetics of AV-45 in rat plasma and metabolism in liver microsomes by ultra-performance liquid chromatography with mass spectrometry. Biomed Chromatogr 2012;26:666–71.
[31] Kuchar M, Mamat C. Methods to increase the metabolic stability of (18)F-radiotracers. Molecules 2015;20:16186–220.
[32] Russak EM, Bednarczyk EM. Impact of deuterium substitution on the pharmacokinetics of pharmaceuticals. Ann Pharmacother 2019;53:211–6.
[33] Pirali T, Serafini M, Cargnin S, Genazzani AA. Applications of deuterium in medicinal chemistry. J Med Chem 2019 [In press].
[34] Schmidt C. First deuterated drug approved. Nat Biotechnol 2017;35:493–4.
[35] Rami-Mark C, Eberherr N, Berroterán-Infante N, Vanicek T, Nics L, Lanzenberger R, et al. [18F] FMeNER-D2: a systematic in vitro analysis of radio-metabolism. Nucl Med Biol 2016;43:490–5.
[36] Nag S, Fazio P, Lehmann L, Kettschau G, Heinrich T, Thiele A, et al. In vivo and in vitro characterization of a novel MAO-B inhibitor radioligand, 18F-labeled deuterated fluorodeprenyl. J Nucl Med 2016;57:315–20.
[37] Liu F, Choi SR, Zha Z, Ploessl K, Zhu L, Kung HF. Deuterated (18)F-9-O-hexadeutero-3-fluoropropoxyl-( )-dihydrotetrabenazine (D6-FP-( )-DTBZ): a vesicular monoamine transporter 2 (VMAT2) imaging agent. Nucl Med Biol 2018;57:42–9.
[38] Liu F, Zhu L, Choi SR, Plossl K, Zha Z, Kung HF. Deuterium-substituted 2-(2′-((dimethylamino)methyl)-4′-[(18) F](fluoropropoxy)phenylthio)benzenamine as a serotonin transporter imaging agent. J Labelled Comp Radiopharm 2018;61:576–85.
[39] Trembath L, Newell M, Devous Sr MD. Technical considerations in brain amyloid PET imaging with 18F-florbetapir. J Nucl Med Technol 2015;43:175–84.

[40] Lemaire C, Plenevaux A, Aerts J, Del Fiore G, Brihaye C, Le Bars D, et al. Solid phase extraction - an alternative to the use of rotary evaporators for solvent removal in the rapid formulation of PET radiopharmaceuticals. J Label Compd Radiopharm 1999;42:63–75.
[41] Zhou D, Chu W, Peng X, McConathy J, Mach RH, Katzenellenbogen JA. Facile purification and click labeling with 2-[(18)F]fluoroethyl azide using solid phase extraction cartridges. Tetrahedron Lett 2015;56:952–4.
[42] Kuge Y, Nishijima K, Nagatsu K, Seki K, Ohkura K, Tanaka A, et al. Chemical impurities in [18F]FDG preparations produced by solid-phase 18F-fluorination. Nucl Med Biol 2002;29:275–9.
[43] Wester H-J, Schoultz BW, Hultsch C, Henriksen G. Fast and repetitive in-capillary production of [18 F] FDG. Eur J Nucl Med Mol Imaging 2009;36:653.
[44] Kovac M, Miklovicz T, Li L, Russell J, Canales Candela R, Aigbirhio F, et al. A simple and efficient automated cGMP-compliant radiosynthesis of [(11) C]metomidate using solid phase extraction cartridge purification. J Labelled Comp Radiopharm 2019;62:190–7.
[45] Mueller D, Klette I, Kalb F, Baum RP. Synthesis of O-(2-[18F]fluoroethyl)-L-tyrosine based on a cartridge purification method. Nucl Med Biol 2011;38:653–8.
[46] Vaulina D, Nasirzadeh M, Gomzina N. Automated radiosynthesis and purification of [(18)F]flumazenil with solid phase extraction. Appl Radiat Isot 2018;135:110–4.
[47] Liu Y, Zhu L, Plössl K, Choi SR, Qiao H, Sun X, et al. Optimization of automated radiosynthesis of [18F] AV-45: a new PET imaging agent for Alzheimer's disease. Nucl Med Biol 2010;37:917–25.
[48] Qu W, Kung M-P, Hou C, Oya S, Kung HF. Quick assembly of 1, 4-diphenyltriazoles as probes targeting β-amyloid aggregates in Alzheimer's disease. J Med Chem 2007;50:3380–7.
[49] Henriksen G, Yousefi BH, Drzezga A, Wester HJ. Development and evaluation of compounds for imaging of beta-amyloid plaque by means of positron emission tomography. Eur J Nucl Med Mol Imaging 2008;35(Suppl. 1):S75–81.
[50] Zha Z, Choi SR, Ploessl K, Lieberman BP, Qu W, Hefti F, et al. Multidentate (18)F-polypegylated styrylpyridines as imaging agents for Abeta plaques in cerebral amyloid angiopathy (CAA). J Med Chem 2011;54:8085–98.
[51] Hamacher K, Coenen HH, Stöcklin G. N.C.A. radio-fluorination of spiperone and N-methylspiperone via aminopolyether supported direct nucleophilic substitution. J Label Compd Radiopharm 1986;23:1047.
[52] Alexoff DL, Casati R, Fowler JS, Wolf AP, Shea C, Schlyer DJ, et al. Ion chromatographic analysis of high specific activity 18FDG preparations and detection of the chemical impurity 2-deoxy-2-chloro-D-glucose. Int J Rad Appl Instrum A 1992;43:1313–22.
[53] Nakao R, Ito T, Yamaguchi M, Suzuki K. Simultaneous analysis of FDG, ClDG and Kryptofix 2.2.2 in [18F]FDG preparation by high-performance liquid chromatography with UV detection. Nucl Med Biol 2008;35:239–44.
[54] Zha Z, Ploessl K, Alexoff D, Choi S, Wu Z, Zhu L, et al. [18F] D3FSP ([18F] D3AV-45) as a PET imaging agent for Abeta plaques in the brain. J Nucl Med 2018;59:1031.
[55] Yao CH, Lin KJ, Weng CC, Hsiao IT, Ting YS, Yen TC, et al. GMP-compliant automated synthesis of [(18)F]AV-45 (Florbetapir F 18) for imaging beta-amyloid plaques in human brain. Appl Radiat Isot 2010;68:2293–7.